Pergamon

Int. J. Heat Mass Transfer. Vol. 39, No. 12, pp. 2427–2447, 1996

0017-9310/96 $15.00 + 0.00

0017-9310(95)00342-8

Spherical vapor bubble growth in uniformly superheated liquids

HO SUNG LEE and HERMAN MERTE, JR†

Department of Mechanical Engineering and Applied Mechanics, The University of Michigan, Ann Arbor, MI 48109-2125, U.S.A.

(*Received* 30 *March* 1995 *and in final form* 12 *September* 1995)

Abstract—A numerical procedure is presented for the solution of vapor bubble growth with radial symmetry from the thermodynamic critical size in an initially uniformly superheated liquid, which includes the influences of surface tension, liquid inertia and heat diffusion. Results are presented in the form of time varying interface radius, velocity, acceleration and temperature, with particular emphasis on how circumstances during the very early growth periods affect the later growth. The effect on the solution of the disturbance required to initiate the growth is examined in some detail. Comprehensive comparisons are made with previous experiments, analyses and numerical results. Copyright © 1996 Elsevier Science Ltd.

1. INTRODUCTION

The prediction of vapor bubble growth involves surface tension, liquid inertia and heat diffusion, and has been the subject of extensive study since the 1930s. As is well known, two intrinsic difficulties are encountered in analytical solutions in which the coupling of the momentum and energy equations are included: the nonlinear convection term in the energy equation, and the linking of the vapor pressure in the momentum equation with the vapor bubble wall temperature in the energy equation. It would seem that this problem has been resolved to a tenable degree of understanding when note is taken of the scarcity of related publications since the work of Prosperetti and Plesset [1].

Following the review of prior works, to be presented below, it was deemed desirable to re-examine the problem of spherical vapor bubble growth. In addition to the lack of a detailed description of the early stages of vapor bubble growth from the critical size, a criterion is lacking as to the circumstances under which the various analytical solutions currently available can be used with confidence, for fluids with widely varying properties, and over wide ranges of system pressure and initial liquid superheat. It is an objective of the present work to provide not only a complete description of the spherical vapor bubble growth, for initially uniform liquid superheats here, but to demonstrate the domains of validity for the analytical solutions currently available and a procedure for the appropriate selection.

2. PRIOR WORKS

Rayleigh [2] was the first to formulate the equation of motion for a spherical bubble growth (or collapse), which was later to be known as the inertia controlled growth. Plesset and Zwick [3] considered the heat diffusion controlled spherical vapor bubble growth neglecting liquid inertia, and provided a zero-order solution for the bubble wall temperature with the assumption of a thin thermal boundary layer, necessary to make the problem tractable. This solution has been widely used in numerical computation of bubble growth for coupling with the equation of motion of Rayleigh [2]. Plesset and Zwick [3] also provided an asymptotic solution for the bubble radius from the zero-order solution which is in good agreement with the experimental data of Dergarabedian [4] with water for moderate superheats up to 6°C. The analyses of Forster and Zuber [5] and Birkhoff *et al.* [6] were basically in agreement with that of Plesset and Zwick [3]. Scriven [7] solves the energy equation without assuming a thin thermal boundary layer, and the asymptotic solution for moderate superheat was identical to that of Plesset and Zwick [3]. The experiments of Kosky [8] for high superheat up to 36°C and the short term microgravity experiments of Florschuetz *et al.* [9] for a superheat of 3.6°C are also in good agreement with the asymptotic solution of Plesset and Zwick [3]. The analytical solutions described to this point may be classified as thermal diffusion controlled growth.

Inertia controlled growth was considered thereafter by Lien [10] in the conduct of low pressure experiments up to 0.01 atm with water. It was concluded that liquid inertia is of significance under low pressure conditions, with heat diffusion coming to dominate growth as the pressure increases, provided that the Rayleigh [2] solution fitted the experiments well at very low pressure.

Mikic *et al.* [11] effectively combined the inertia and heat diffusion controlled growth by using the

† Author to whom correspondence should be addressed.

NOMENCLATURE

c	specific heat	ΔT	$(T_\infty - T_{sat})$, bulk liquid superheat
h_{fg}	latent heat	ΔP	$P_v - P_\infty$
Ja	Jakob number $(= \rho_l c_l (T_\infty - T_{sat})/\rho_v h_{fg})$	u	velocity.
k	thermal conductivity		
P	pressure	Greek symbols	
r	radial coordinate	α	thermal diffusivity
$R(t)$	bubble radius	μ	dynamic viscosity, also defined in equation (11)
R^+	dimensionless radius defined in equation (9)	ρ	density
R^*	dimensionless radius defined in equation (11)	σ	surface tension.
t	time		
t^+	dimensionless time defined in equation (9)	Subscripts	
t^*	dimensionless time defined in equation (11)	d	delay
T	temperature	i	liquid–vapor interface
T_{sat}	saturation temperature corresponding to system pressure	l	liquid
		r	radial
		v	vapor
		∞	infinite or far field.

Clausius–Clapeyron equation for the vapor pressure curve, assuming thermal equilibrium in the vapor bubble so that the vapor pressure corresponds to the bubble wall temperature as the bubble grows. The result was a generalized closed form expression which was valid over the entire growth range, with good agreement with the experimental data of Lien [10].

Theofanous and Patel [12] reconsidered the analysis of Mikic *et al.* [11] relative to the form of the Clausius–Clapeyron equation used, and upon comparison with the measurements of Bohrer [13] demonstrated that the bubble growth is considerably understated. As a result, an empirical linear relation for the vapor-pressure was suggested to replace the Clausius–Clapeyron relation. The adequacy of this linear relation in describing the physical process will be considered in detail later here.

A number of numerical computations were carried out by coupling the equation of motion with various special forms of the energy equation: Theofanous *et al.* [14] used a quadratic temperature distribution in place of the energy equation; Board and Duffey [15] used a one-dimensional (1D) transient conduction prediction; and Prosperetti and Plesset [1] used the zero-order solution mentioned earlier for the bubble wall temperature.

Dalle Donne and Ferranti [16] were among the first to solve the complete equations of energy and motion, using sodium as the medium, with no assumptions being made about the thermal boundary layer at the liquid–vapor interface, as was found necessary by Plesset and Zwick [3]. More accurate details of the early stages of bubble growth were provided.

Although the initial stages of vapor bubble growth are generally considered to be insignificant, since they lie outside time scales of practical interest, numerical treatments require that perturbations be imposed on the critical size vapor bubble to initiate the growth. Theofanous *et al.* [14] initiated the bubble growth with a small pressure perturbation at $t = 0$; Board and Duffey [15] perturbed the equilibrium radius by 0.05%; and both Plesset and Zwick [3] and Dalle Donne and Ferranti [16] introduced an energy generation term in the energy equation. It is uniformly postulated that the perturbations applied do not affect the subsequent vapor bubble growth provided that the perturbations are sufficiently small. The effects of variations in such perturbations will be considered below.

Utilizing the results of Dalle Donne and Ferranti [16] as a basis for comparison, Prosperetti and Plesset [1] reconsidered two facets of earlier analyses: the validity of the assumption of a thin thermal boundary layer, and the effects of using a linear relation for the vapor pressure curve as suggested by Theofanous and Patel [12]. It was demonstrated that the thin thermal boundary layer assumption is fairly good unless extremely low levels of superheat are used, and that the application of the linear relation for the vapor pressure curve tends to somewhat overestimate the bubble growth, especially at high superheat levels. It was stated that this overestimate does not lead to a serious error in the radius-time behavior for ranges of practical interest. A modified form of the expression of Mikic *et al.* [11] was then developed, using the linear relation suggested by Theofanous and Patel [12], with the recognition that these analytical solutions can not correctly describe the early or surface

tension dominated stages of growth, which in any case may not be of practical interest.

To assist in the assessment of prior analytical solutions with respect to the complete solutions presented here, the relationship developed in these prior works will be given in brief below.

3. ANALYTICAL SOLUTIONS OF PRIOR WORKS

Rayleigh [2] formulated the equation of motion as:

$$R\frac{d^2R}{dt^2}+\frac{3}{2}\left(\frac{dR}{dt}\right)^2=\frac{P_v-P_\infty}{\rho_l}. \tag{1}$$

A surface tension term is added later by Plesset and Zwick [3] as:

$$R\frac{d^2R}{dt^2}+\frac{3}{2}\left(\frac{dR}{dt}\right)^2=\frac{P_v-P_\infty}{\rho_l}-\frac{2\sigma}{\rho_l R}. \tag{2}$$

Assuming that the pressure difference (P_v-P_∞) is constant, equation (1) can be solved for dR/dt:

$$\frac{dR}{dt}=\left(\frac{2(P_v-P_\infty)}{3\rho_l}\right)^{1/2}. \tag{3}$$

Equation (3) is one form of the so-called inertia controlled growth, and may be considered as an adequate description if the initial superheat is sufficiently large or the system pressure is sufficiently low. Plesset and Zwick [17] derived a zero-order solution for the bubble wall temperature from the energy equation, assuming a thin thermal boundary layer, as

$$T_i=T_\infty-\left(\frac{\alpha}{\pi}\right)^{1/2}\int_0^t\frac{R^2(x)\left(\frac{\partial T}{\partial r}\right)_{r=R(x)}}{\left(\int_x^t R^4(y)\,dy\right)^{1/2}}dx. \tag{4}$$

Plesset and Zwick [3] later derived an asymptotic solution for the bubble growth from this zero-order solution, which is valid only for times sufficiently large that the growth velocity is much smaller than that corresponding to the inertia controlled case, given as:

$$\frac{dR}{dt}=\frac{1}{2}\left(\frac{12\alpha_l}{\pi t}\right)^{1/2}\frac{\rho_l c_l(T_\infty-T_{sat})}{\rho_v h_{fg}}. \tag{5}$$

Mikic *et al.* [11] resolved the complexity of solving the combination of the energy and momentum equations by combining the two growth rate equation limits given by equations (3) and (5), in effect. The form of the Clausius–Clapeyron equation, integrated for constant properties at P_∞ and T_{sat} is:

$$P_v-P_\infty=\frac{\rho_v h_{fg}}{T_{sat}}(T_v-T_{sat}) \tag{6}$$

and is substituted into the inertia dominated growth rate equation (3) to express the driving potential in terms of temperatures rather than pressure, resulting in:

$$\frac{dR}{dt}=\left(\frac{2\rho_v h_{fg}(T_v-T_{sat})}{3\rho_l T_{sat}}\right)^{1/2} \tag{7}$$

T_{sat} in equation (5) was replace by the instantaneous vapor temperature T_v, which retains the physical principles involved, giving:

$$\frac{dR}{dt}=\frac{1}{2}\left(\frac{12\alpha_l}{\pi t}\right)^{1/2}\frac{\rho_l c_l(T_\infty-T_v)}{\rho_v h_{fg}}. \tag{8}$$

Eliminating T_v between equations (7) and (8) and integrating dR/dt yields the closed-form expression of Mikic *et al.* [11] as:

$$R^+=\tfrac{2}{3}[(t^++1)^{3/2}-(t^+)^{3/2}-1] \tag{9}$$

where

$$R^+=\frac{R}{B^2/A}\qquad t^+=\frac{t}{B^2/A^2}$$

$$A=\left(\frac{2\Delta T h_{fg}\rho_v}{3T_{sat}\rho_l}\right)^{1/2}\qquad B=\left(\frac{12}{\pi}Ja^2\alpha_l\right)^{1/2}.$$

Equation (9) simplifies to the Rayleigh solution equation (7) for $t^+\ll 1$ and to the Plesset and Zwick solution equation (8) for $t^+\gg 1$, and is in good agreement with the experiments of Lien [10] with water, except for those at very low pressure.

Theofanous and Patel [12] suggested a modification to the solution of Mikic *et al.* [11] by the use of a linear vapor pressure relation instead of the Clausius–Clapeyron equation, justifying it on the basis of improved comparison with the experiments of Bohrer [13] for R113. The linear relationship proposed is:

$$P_v=P_\infty+\frac{P_v(T_\infty)-P_\infty}{T_\infty-T_{sat}}(T_v-T_{sat}). \tag{10}$$

Prosperetti and Plesset [1] carried out numerical computations by coupling equations (2) and (4), using the exact vapor–pressure curve, with excellent agreement with the numerical results of Dalle Donne and Ferranti [16], except at very low superheats. The discrepancy at low levels of superheat is to be expected, since the assumption of the thin thermal boundary layer is no longer valid. Computations were also carried out by coupling equations (2) and (4) using the linear vapor–pressure relation given by equation (10), with the result that high superheats somewhat overestimate the growth. However, it was stated that this overestimate does not lead to a serious error in the radius–time behavior of vapor bubbles for ranges of practical interest. Consequently, a scaled modified closed-form expression of Mikic *et al.* [11] was provided, adopting the linear vapor–pressure relation, as:

$$R^*=\frac{2}{\pi^2}(2/3)^{1/2}[(\tfrac{1}{2}\pi^2 t^*+1)^{3/2}-(\tfrac{1}{2}\pi^2 t^*)^{3/2}-1] \tag{11}$$

where

$$R^* = \mu^2 \frac{R}{R_c} \quad t^* = \beta\mu^2 t$$

$$\mu = \frac{1}{3}\left(\frac{2\sigma\alpha}{\pi}\right)^{1/2} \rho_v \frac{h_{fg}}{k}(T_\infty - T_{sat})^{-1}$$

$$\times \{\rho_v[P_v(T_\infty) - P_\infty]\}^{-1/4}$$

$$\beta = \frac{[P_v(T_\infty) - P_\infty]^{3/2}}{2\sigma\rho_l^{1/2}}.$$

Comparisons will be provided below between the current predictions and those of Mikic *et al.* [11], equation (9), and of Prosperetti and Plesset [1], equation (11), and therefore, indirectly, between these latter two, for a variety of fluids.

4. CURRENT SOLUTIONS

In order to study the characteristics of spherically symmetric vapor bubble growth in detail, a Fortran program was written, compatible for use on currently available PCs, to model the growth (or collapse) using a highly accurate numerical scheme, taking into account the variations of properties with temperature. The equation of motion and the complete energy equation are solved simultaneously using the vapor–pressure curve. For the infinitesimal time steps, the equation of motion is solved by means of the Runge–Kutta method to determine the locus of the bubble interface, which provides the boundary condition for the energy equation. The complexity of the problem is simplified by adopting the Landau coordinate transformation to immobilize the moving boundary. After the transformation, the energy equation is solved by the finite difference method (FDM) with the aid of the Thomas algorithm, the TriDiagonal Matrix Algorithm. The formulations of the governing equations used in computations are given in Appendix A and details of the numerical solution procedure are given in Appendix B.

4.1. *Initial and early stages of bubble growth*

A spherical vapor bubble is assumed to form and begin its growth from the thermodynamic critical size. This formation is based on homogeneous nucleation theory (e.g. Skripov [18]), such that an increase in the bulk liquid superheat decreases the work of formation of the critical size nucleus and increases the mean level of the energy fluctuations of clusters of liquid molecules. As a result of these factors the nucleus is highly unstable. The vapor pressure in the critical size nucleus is higher than that of the adjacent liquid, and is balanced mechanically by the surface tension. When making numerical computations, a small disturbance is required to initiate the vapor bubble growth from the critical size, which could be interpreted as a fluctuation in temperature or pressure at the liquid–vapor interface. In the computational process here a vapor temperature slightly higher than the initial bulk temperature is imposed, for the initial time step only, to provide the disturbance necessary for growth to begin, expressed as:

$$T_v = T_\infty + \Delta T_{disturb}. \tag{12}$$

Computations of bubble radius and interface velocity are presented in Fig. 1 to demonstrate the effects of the magnitude of the initial disturbance, for water at atmospheric pressure and superheats of 3.1°C and 36°C. In the early period, when the forces are nearly in equilibrium, the growth is imperceptibly small, but accelerates with increases in bubble size as the surface tension reduces. The time interval between the imposed disturbance and where the bubble radius undergoes a perceptible change is defined as the bubble growth delay time (t_d), and varies depending on the magnitude of the disturbance. Two general conclusions might be deduced for the sample computations presented in Fig. 1, in which temperature disturbances of 10^{-1}, 10^{-5} and 10^{-9}°C were used. For the high and moderate superheat levels in Fig. 1, the bubble growth delay times are below time periods of practical interest, and converge quickly to an asymptotic value, as demonstrated in Fig. 2. An arbitrary initial temperature disturbance of 10^{-4}°C is used in all computations presented hereafter. For reference purposes it might be noted that a temperature disturbance of 10^{-5}°C in the vapor temperature corresponds to the energy content of seven molecules out of a total of approximately 107 in a critical size vapor bubble in water at atmospheric pressure superheated by 36°C. The other conclusion to be noted in Fig. 1 is that the subsequent bubble growth is uninfluenced by differences in the disturbance, beginning at 10^{-3} s and 10^{-5} s for superheats of 3.1°C and 36°C, respectively.

The maximum liquid–vapor interface velocity in Fig. 1 is about 10 m s^{-1} for a superheat of 36°C, considerably less than the sonic velocity, so that the assumption of a uniform pressure in vapor bubble is justified. Even for an extreme case of 100°C superheat at a pressure of 4 atm, computation provided a maximum liquid–vapor interface velocity of only 35 m s^{-1}. A small dip on the interface velocity curve in Fig. 1 occurs at about 10^{-5} s for the superheat of 3.1°C, and is related to the relative effects of surface tension and pressure difference between the bubble vapor and bulk liquid. This phenomena is examined in detail by Lee [19]. The computed liquid–vapor interface accelerations corresponding to the identical conditions of Fig. 1 are shown in Fig. 3. Even a relatively small superheat of 3.1°C produces an enormous acceleration of 2×10^4 s^{-2}, albeit of short duration. The bubble wall accelerates as the equilibrium of surface tension is removed, but is limited by the adverse liquid inertia. The subsequent decrease of the interface acceleration to negative values is a consequence of the inability of the vapor production rate to match the early growth rates seen in Fig. 1. The deceleration eventually approaches zero asymptotically. It is here

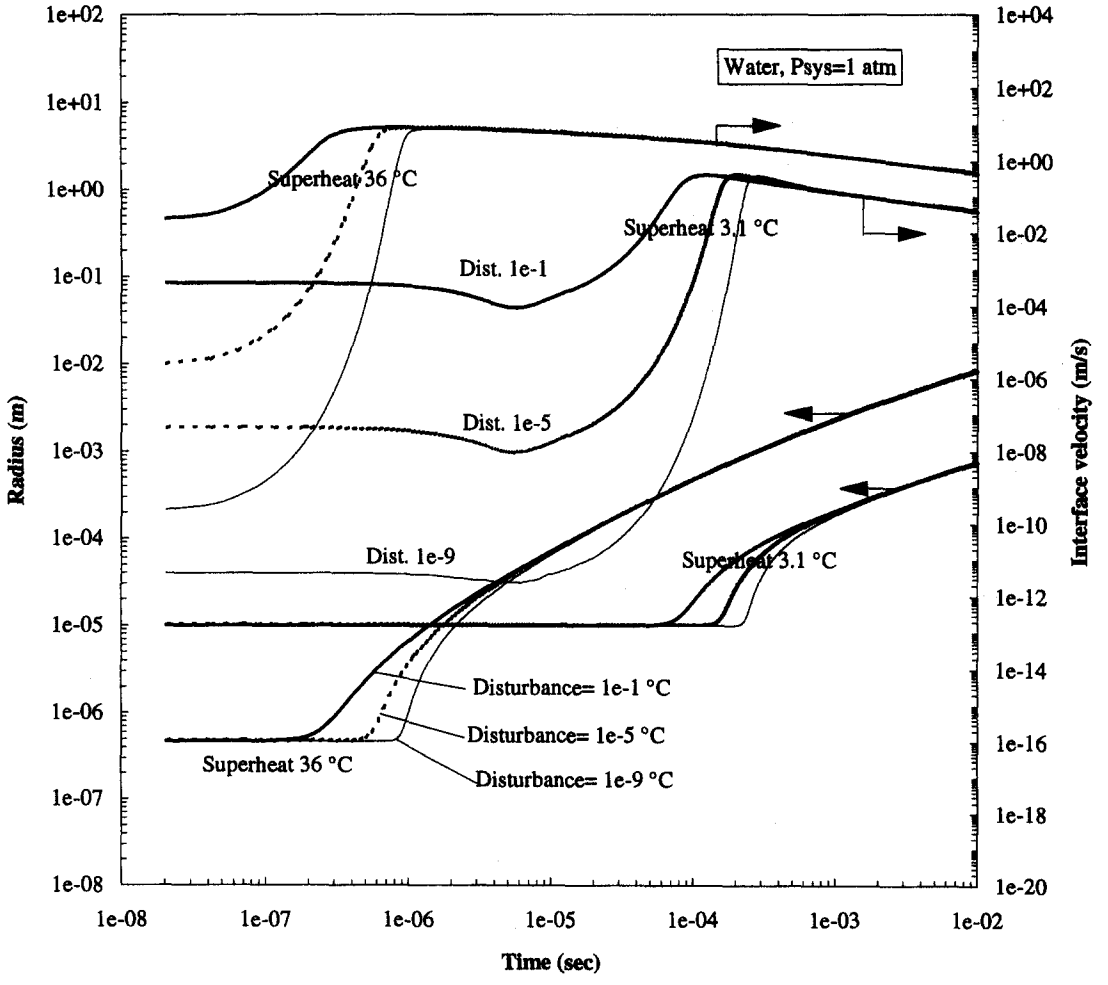

Fig. 1. Influence of magnitude of initial temperature disturbance on the early vapor bubble growth for water at atmospheric pressure.

that the bubble growth is then controlled by thermal diffusion, which some models successfully describe, as amplified in the next section. It is also to be noted in Fig. 3 that no significant changes in peak acceleration occur as the disturbance is varied. Since the early stages of bubble growth are affected by both surface tension and liquid inertia, as well as by the magnitude of the disturbance required, it is not unexpected that difficulties arise in obtaining analytical solutions. Calculated results demonstrate the well-known phenomena that the thermal boundary layer thickness increases continuously with time.

4.2. *Comparison with other works*

In order to assess the adequacy of the computational model developed here, comparisons will now be made with previous experiments, analyses and numerical results.

The measurement of water vapor bubbles at the thermodynamic critical size involves insurmountable experimental difficulties at present for moderate and high levels of liquid superheat. However, creative experimental techniques of Dergarabedian [20] provided measurements of bubble growth in water at atmospheric pressure with low levels of liquid superheat, which included measurements of the thermodynamic critical size. These measurements are plotted in Fig. 4, along with values computed by the procedures described above for liquid superheats of 0.8°C and 1.0°C. The time origins for the computations were shifted for the best fit by selecting arbitrary values of 10^{-4}°C and 10^{-9}°C for the respective disturbances. To be contrasted with the behavior demonstrated in Fig. 1, where the magnitude of the disturbances have negligible effect on measurable bubble growths at moderate and high bulk liquid superheat levels, the disturbance does influence the measurable levels at low levels of superheat.

The present computations are compared with measurements of Lien [10] in Fig. 5 for water at various subatmospheric pressure levels, with reasonably good agreement.

Comparisons of the vapor bubble sizes between the current computations and a number of previous

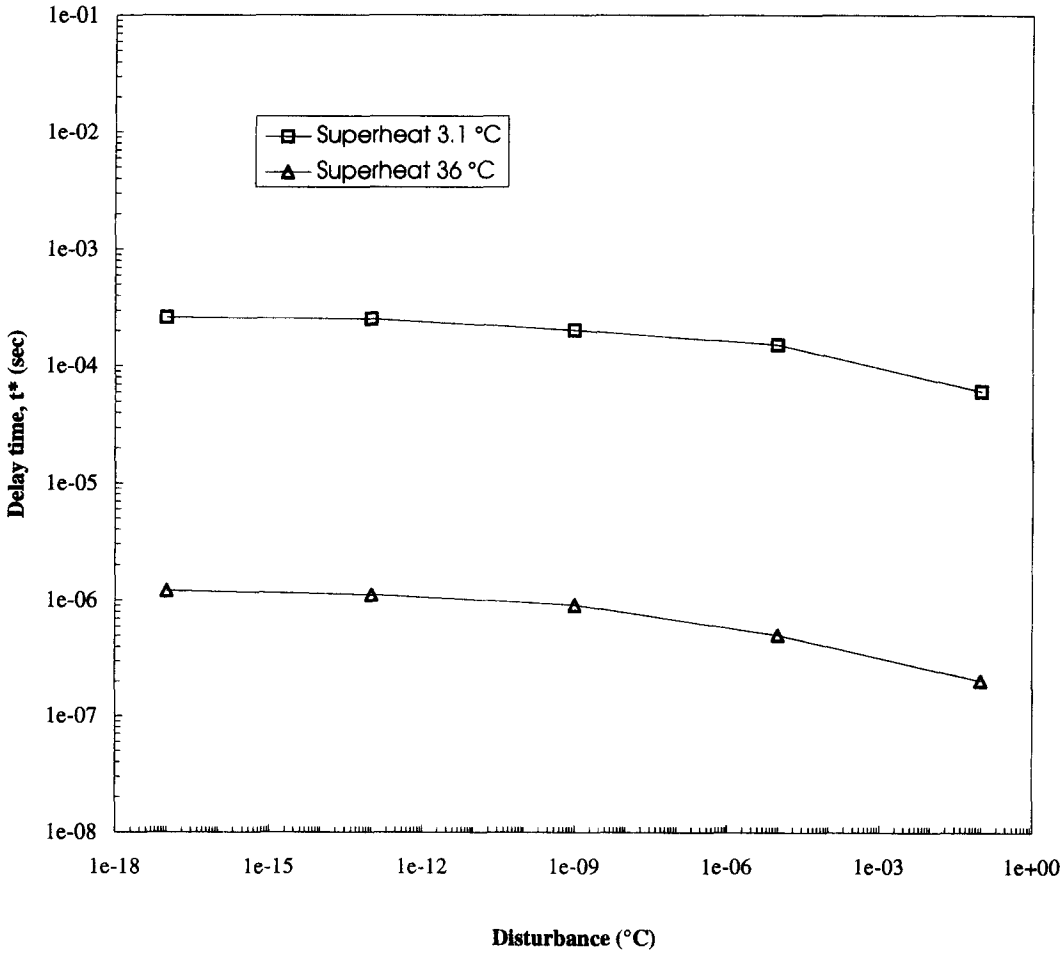

Fig. 2. Effect of initial temperature disturbance on bubble growth delay time for water.

analyses are given in Figs. 6 and 7 for water at atmospheric pressure and a relatively higher superheat of 36°C, the same condition used in Figs 1 and 3. The Rayleigh curve denotes the inertia controlled growth, with the corresponding most rapid growth. The time periods covered are identical, while the behavior during the very early periods is amplified in Fig. 7 by the use of logarithmic scales. The consequence of neglecting surface tension is evident during the early bubble growth period, as had been anticipated in discussions associated with the prior analyses. The relationship between the analyses of Mikic *et al.* [11] and of Prosperetti and Plesset [1] will be considered in some detail below.

The present computations produce excellent agreement with the numerical work of Dalle Donne and Ferranti [16] for various superheats and system pressure in sodium. A typical result is shown in Fig. 8. Two major differences exist between the present work and that of Dalle Donne: (1) the former uses the Landau transformation while the latter uses the Lagrange transformation to immobilize the moving boundary, (2) the former uses a temperature disturbance for one time step only at the liquid–vapor interface at the beginning of the computation process, while the latter uses a constant energy source during the entire computation period to initiate the bubble growth from the condition of metastable equilibrium.

4.3. *General characteristics of bubble growth*

In order to illustrate the relative effects of liquid inertia, surface tension, heat diffusion and vapor pressure on vapor bubble growth, three fluids having rather divergent properties were selected for more detailed examination: water, R-113 and sodium. Figures 9 and 10 present results obtained with the current numerical procedure for a high superheat of 36°C and at atmospheric pressure. Figure 9 gives the radius and liquid–vapor interface velocity vs time, and Fig. 10 presents the interface acceleration and vapor pressure. It is noted that the maximum interface velocities and peak acceleration levels are not significantly different between the three fluids, although the sizes at 0.1 s differ by two orders, associated with the time variation of the interface velocities. Furthermore, the bubble growth delay time is considerably greater for the sodium than for the R-113 and water, owing to its relative large thermal diffusivity. The same initial tem-

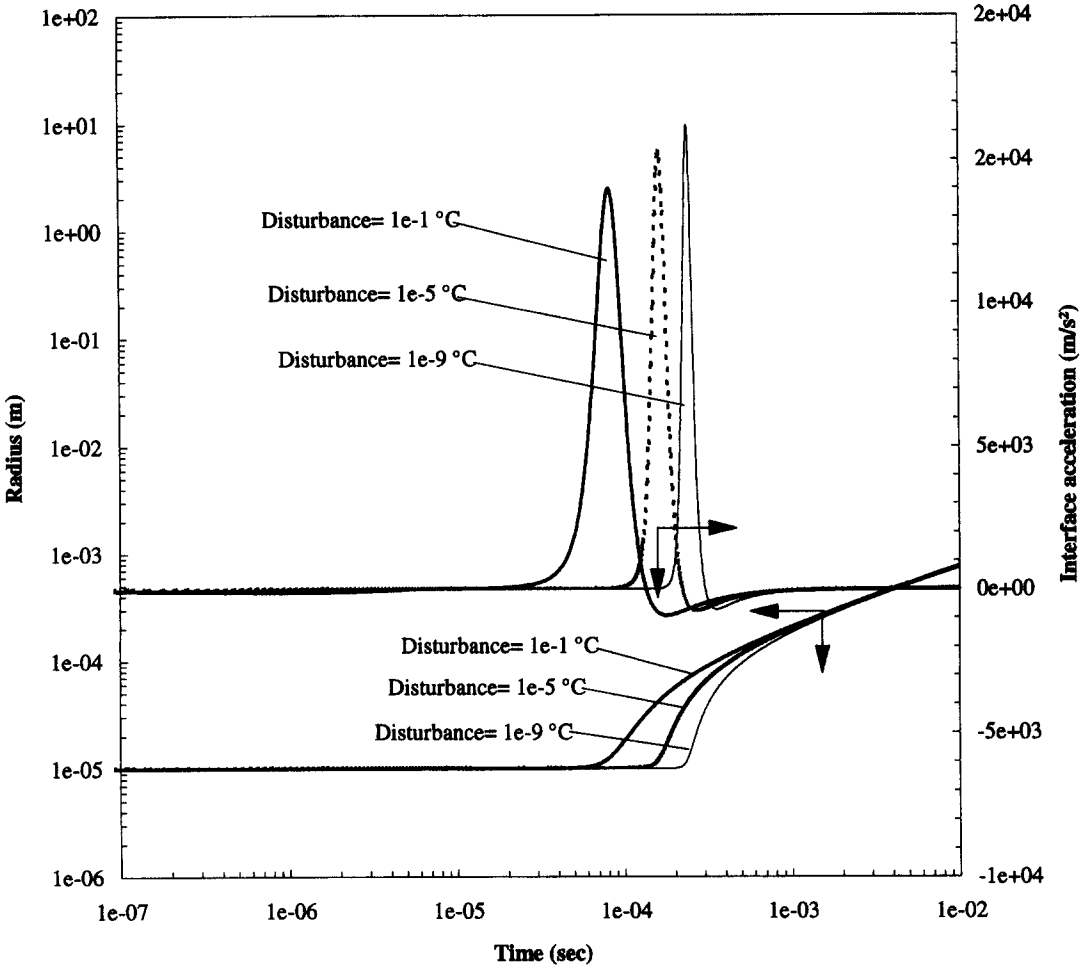

Fig. 3. Influence of magnitude of initial temperature disturbance on the early liquid vapor interface acceleration. Water at atmospheric pressure at initial superheat of 3.1°C.

perature disturbance of 10^{-4}°C is used for each of the fluids. The initial vapor pressures given in Fig. 10 correspond to the initial bulk temperature, with the pressure for water R-113 dropping rapidly to the system pressure at about 1×10^{-3} s, while for sodium this occurs at about 1×10^{-2} s.

In order to compare the analytical solutions of Mikic *et al.* [11] and Prosperetti and Plesset [1] with the results of the present numerical computations, the radii and velocities in Fig. 9 were normalized using the respective nondimensional definitions, and are plotted as Figs 11 and 12, respectively. As demonstrated in Fig. 11, the radius and velocity curves converge quite well to the solution of Mikic *et al.* [11] except for the early stage of growth. On the other hand, the modified solution by Prosperetti and Plesset [1] in Fig. 12 overestimates the vapor bubble growth by about 43%.

As described earlier, the only difference between the solutions of Mikic *et al.* [11] and Prosperetti and Plesset [1] is that the former uses the integrated form of the Clausius–Clapeyron equation (6), with constant properties evaluated at the saturation temperature, while the latter uses the linear relation, equation (10). The distinction between the use of these forms and the true vapor pressure curve is illustrated graphically in Fig. 13. The relations between the internal bubble vapor pressure and vapor temperature proceed as indicated by the arrows. It becomes obvious that for a given system temperature the integrated Clapeyron equation underestimates the vapor pressure while the linear relation overestimates it. The underestimation of the Clapeyron equation is substantial in the beginning at T_∞, but converges to the exact curve as the bubble grows and T_∞ approaches T_{sat}, while the linear relation matches both the beginning and the end. Additional comparisons similar to Figs 11 and 12 were conducted for these fluids, covering superheats from 3°C to 100°C and system pressures from 0.1 atm and 6 atm. A maximum error of 39% was obtained between the bubble size computed by the solution of Mikic *et al.* [11] and by the present procedure, and

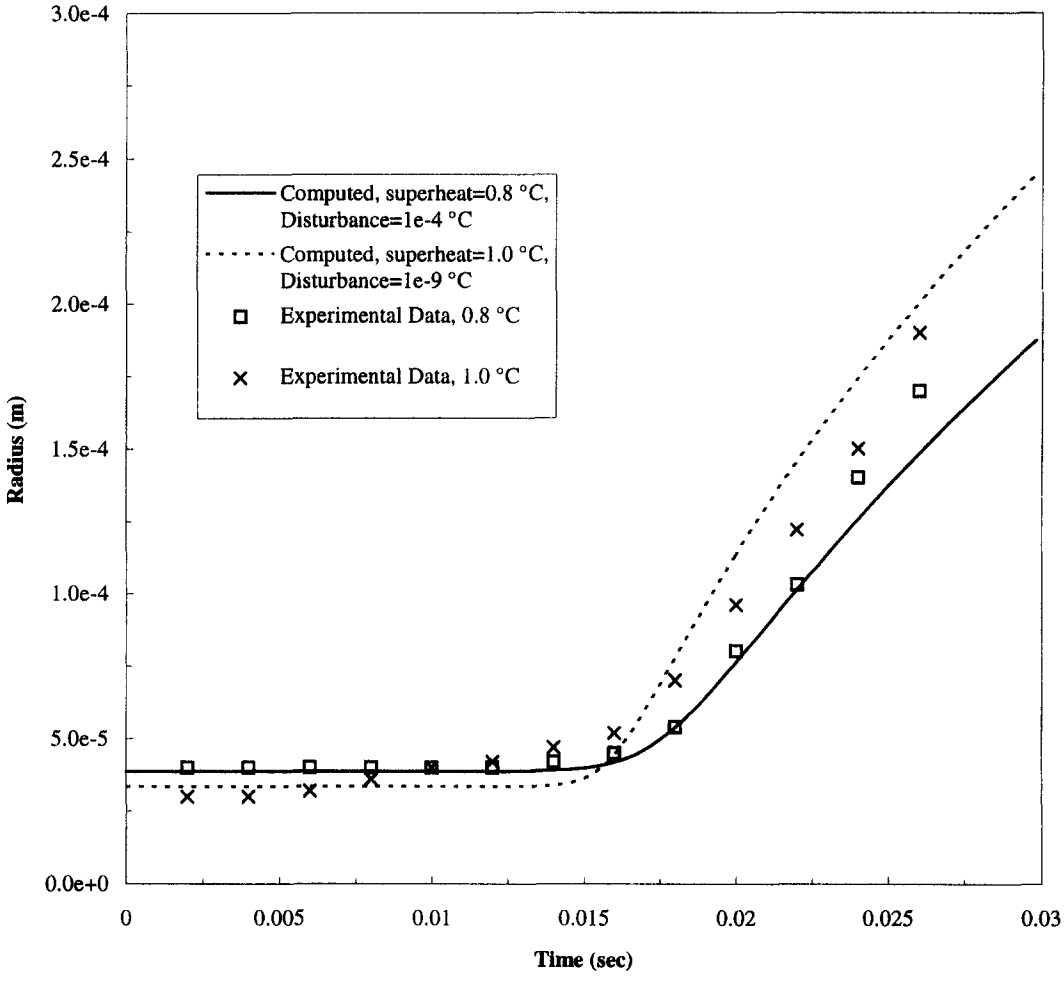

Fig. 4. Comparison of computations of vapor bubble growth with measurements of Dergarabedian [20] for water at atmospheric pressure with low initial liquid superheats.

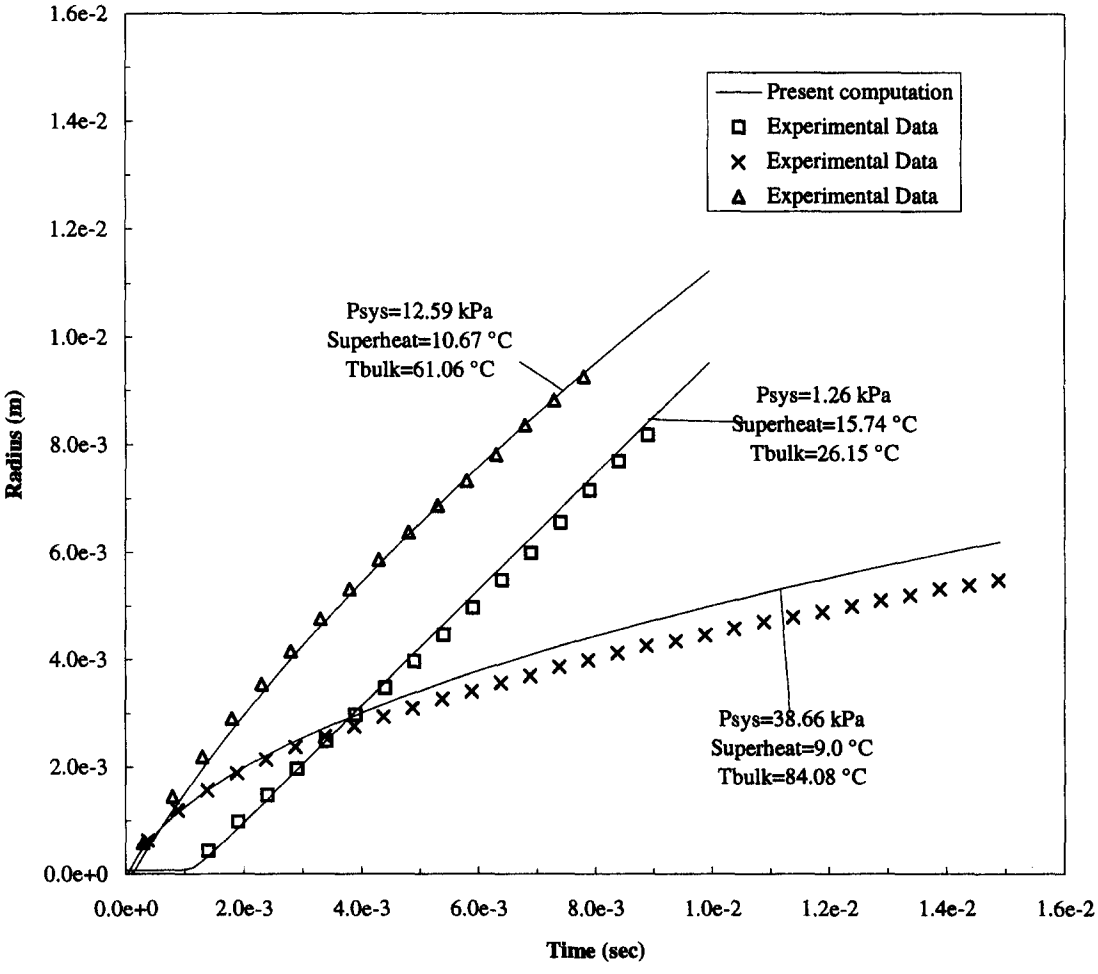

Fig. 5. Comparison of present numerical calculations with measurements of Lien [10] with water over a range of subatmospheric pressure levels.

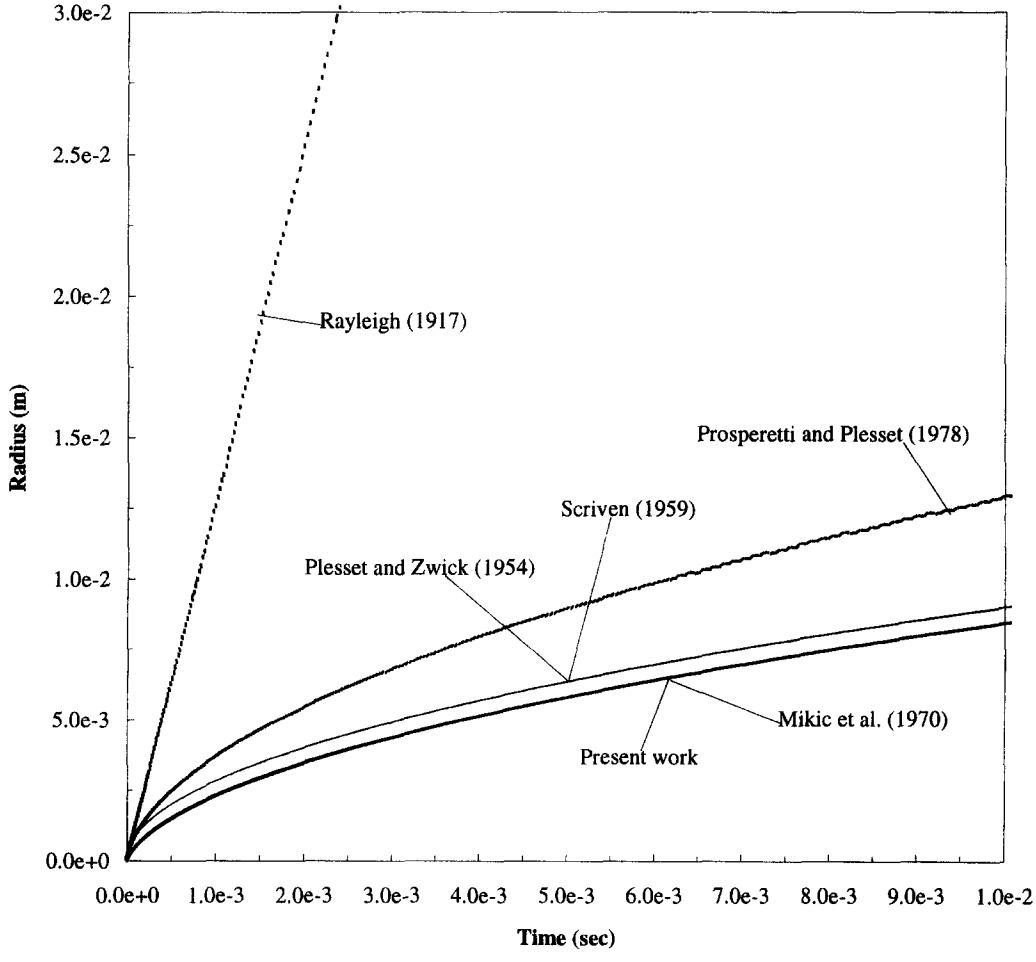

Fig. 6. Comparison of present numerical calculations with various analytical solutions. Water at atmospheric pressure uniformly superheated to 36°C, $Ja = 110$.

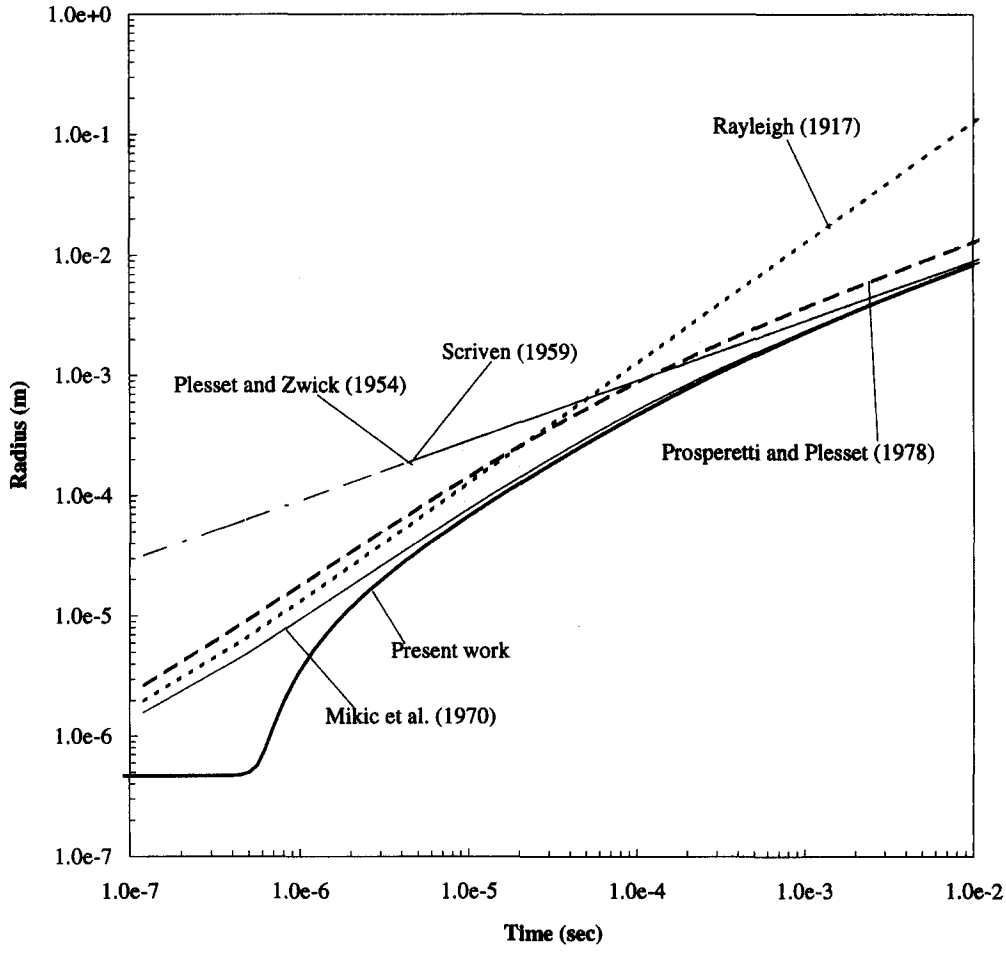

Fig. 7. Comparison of present numerical calculations with various analytical solutions. Water at atmospheric pressure uniformly superheated to 36°C, $Ja = 110$. The early period of Fig. 6 is amplified with the use of logarithmic axes.

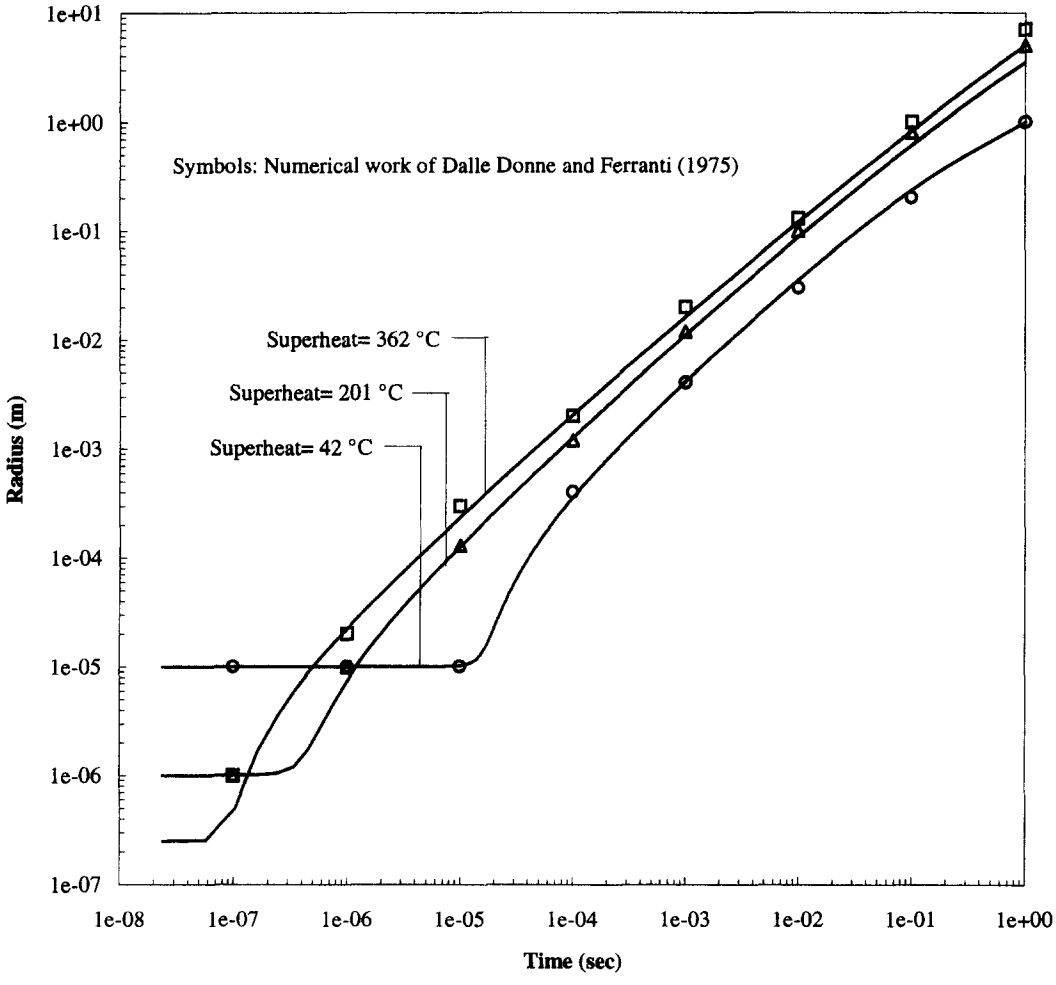

Fig. 8. Comparisons of present computed results with the numerical work of Dalle Donne and Ferranti [5], for sodium at pressure of 0.5 atmosphere.

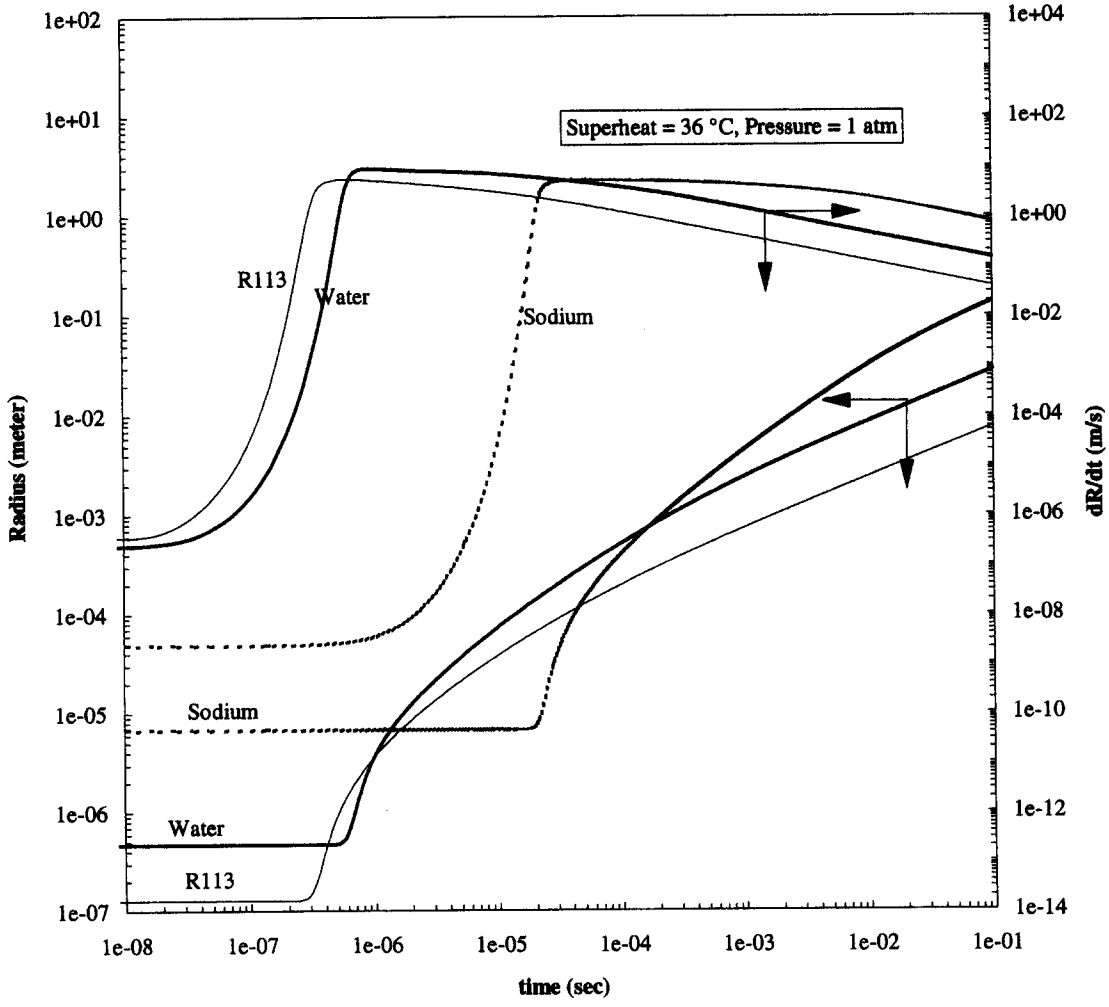

Fig. 9. Comparisons of computed bubble radius and liquid–vapor interface velocity vs time for water, R-113 and sodium all at atmospheric pressure and a high superheat of 36°C.

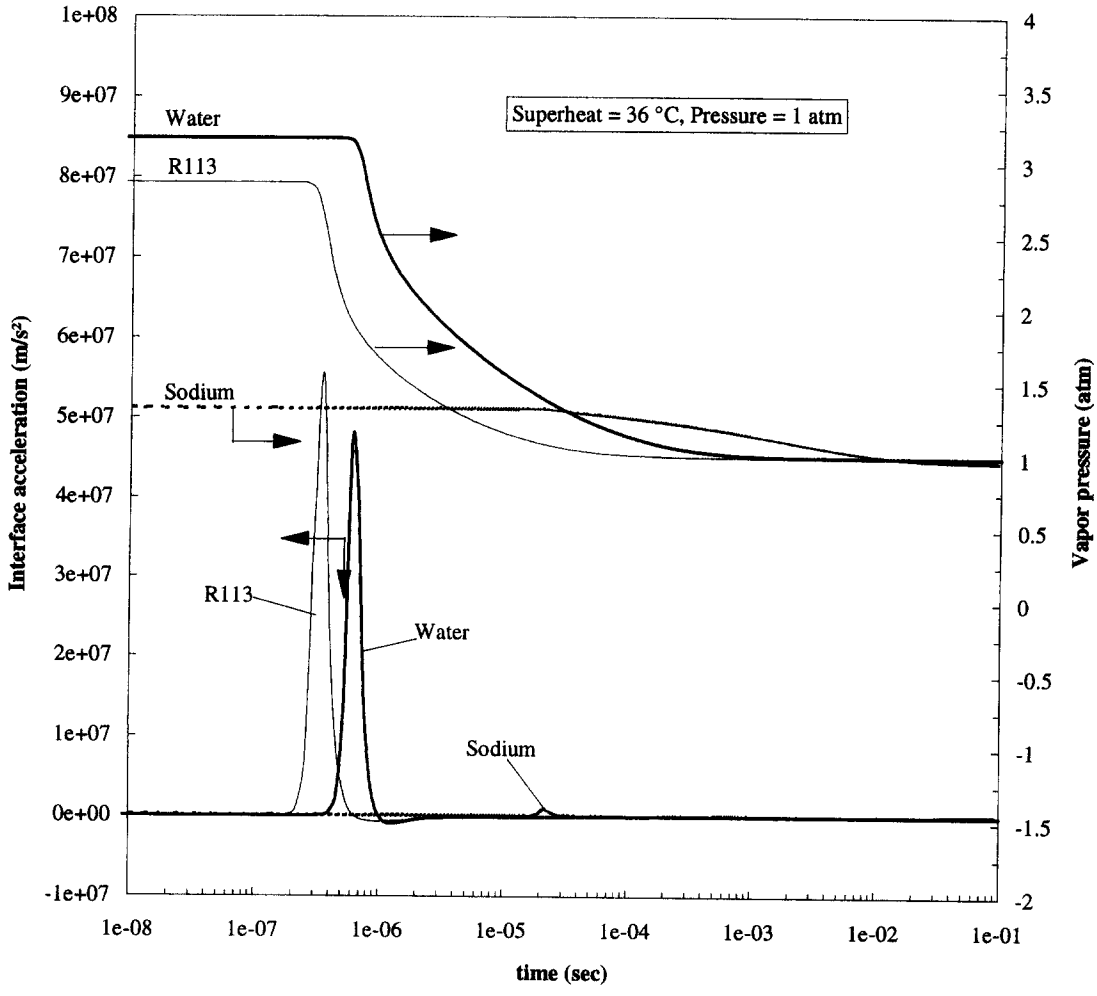

Fig. 10. Comparisons of interface acceleration and vapor pressure vs time for conditions identical to those given in Fig. 9.

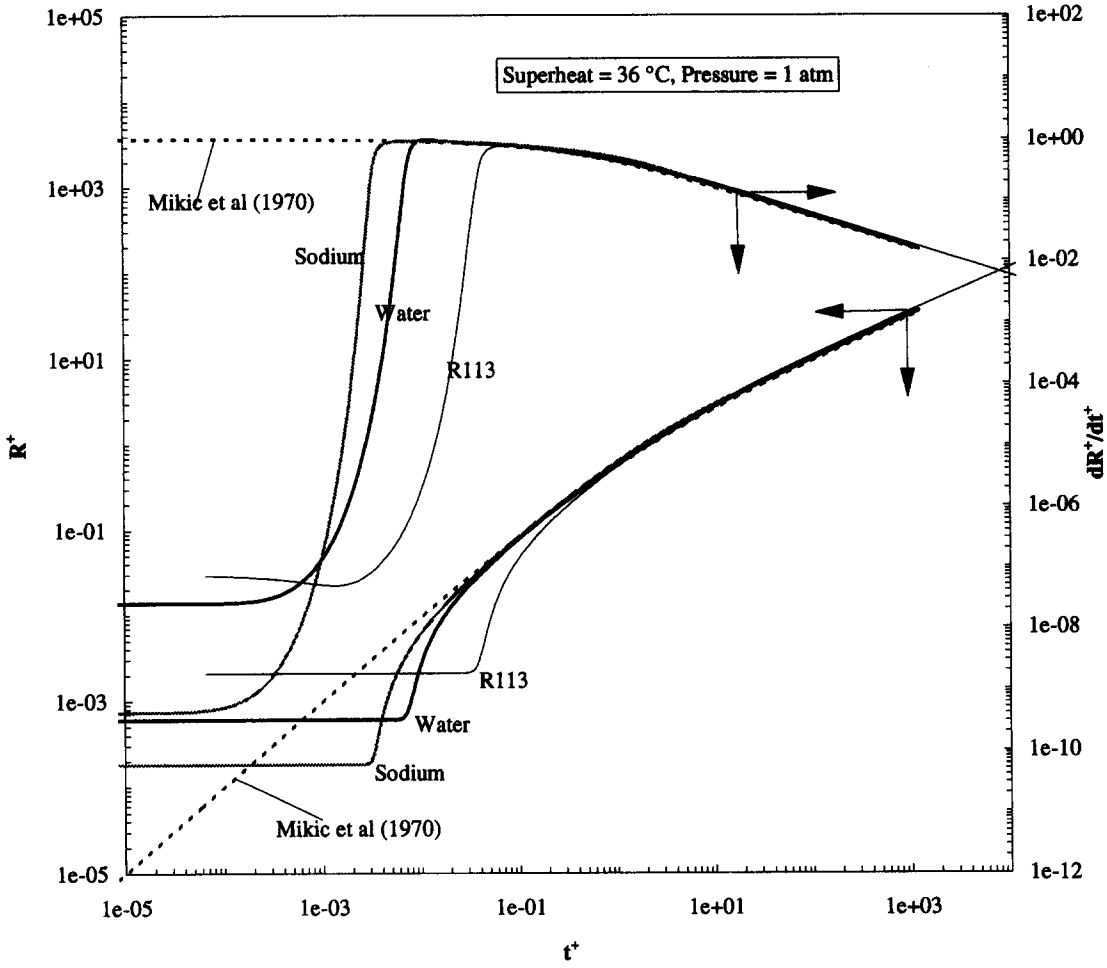

Fig. 11. Comparisons of nondimensional forms of bubble radius and liquid–vapor interface velocity for the three fluids from Fig. 9 with the analytical solution of Mikic *et al.* [11], equation (9).

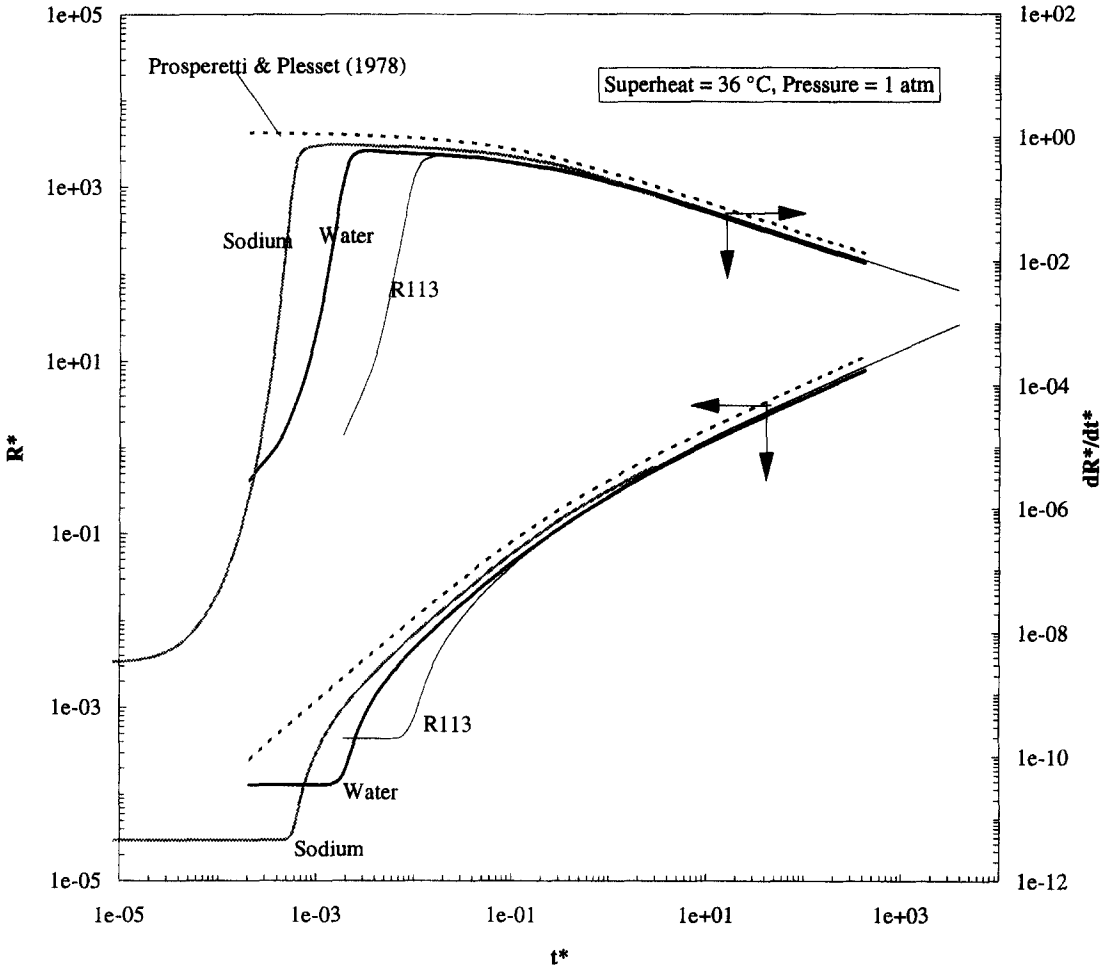

Fig. 12. Comparisons of nondimensional forms of bubble radius and liquid–vapor interface velocity for the three fluids from Fig. 9 with the analytical solution of Prosperetti and Plesset [1], equation (11).

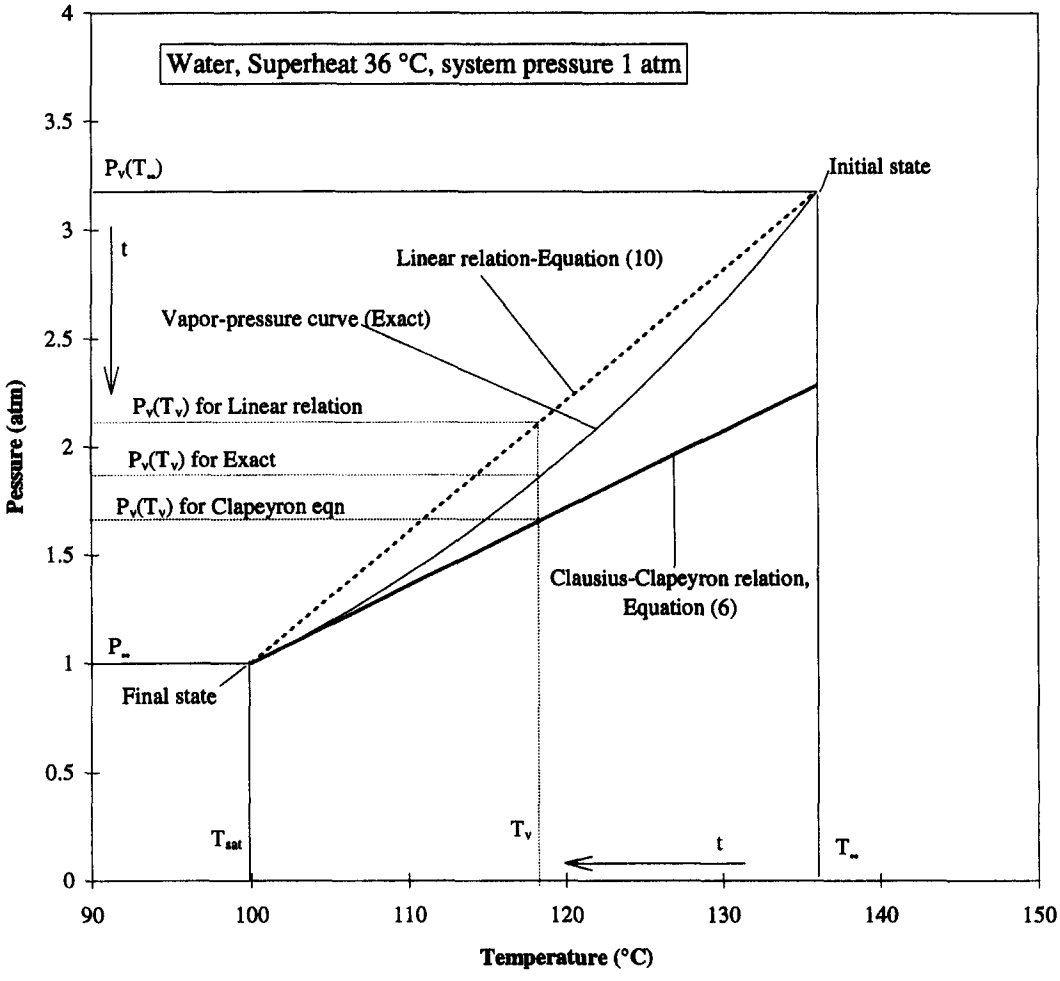

Fig. 13. Comparisons between the vapor pressure and approximations determined by the integrated Clausius–Clapeyron relation and a linear interpolation function.

then only with R-113 for a superheat of 100°C at 1 atm. It is found that the modified solution of Prosperetti and Plesset [1] always overestimates the bubble size considerably, the more so as either the superheat increases or the pressure decreases. For a superheat of 36°C and pressure of 0.1 atm the error is about 74%, while for a superheat of 100°C at 1 atm pressure this increases to about 160%. The integrated Clapeyron equation works well in the solution of Mikic *et al.* [11] even though Fig. 13 shows a discrepancy compared to the exact vapor pressure curve because the vapor pressure (P_v) decreases rapidly during the early bubble growth period, within about 1 ms as seen in Fig. 10, to the system pressure (P_∞).

In order to more specifically classify the domains in which liquid inertia and heat diffusion effects domi-

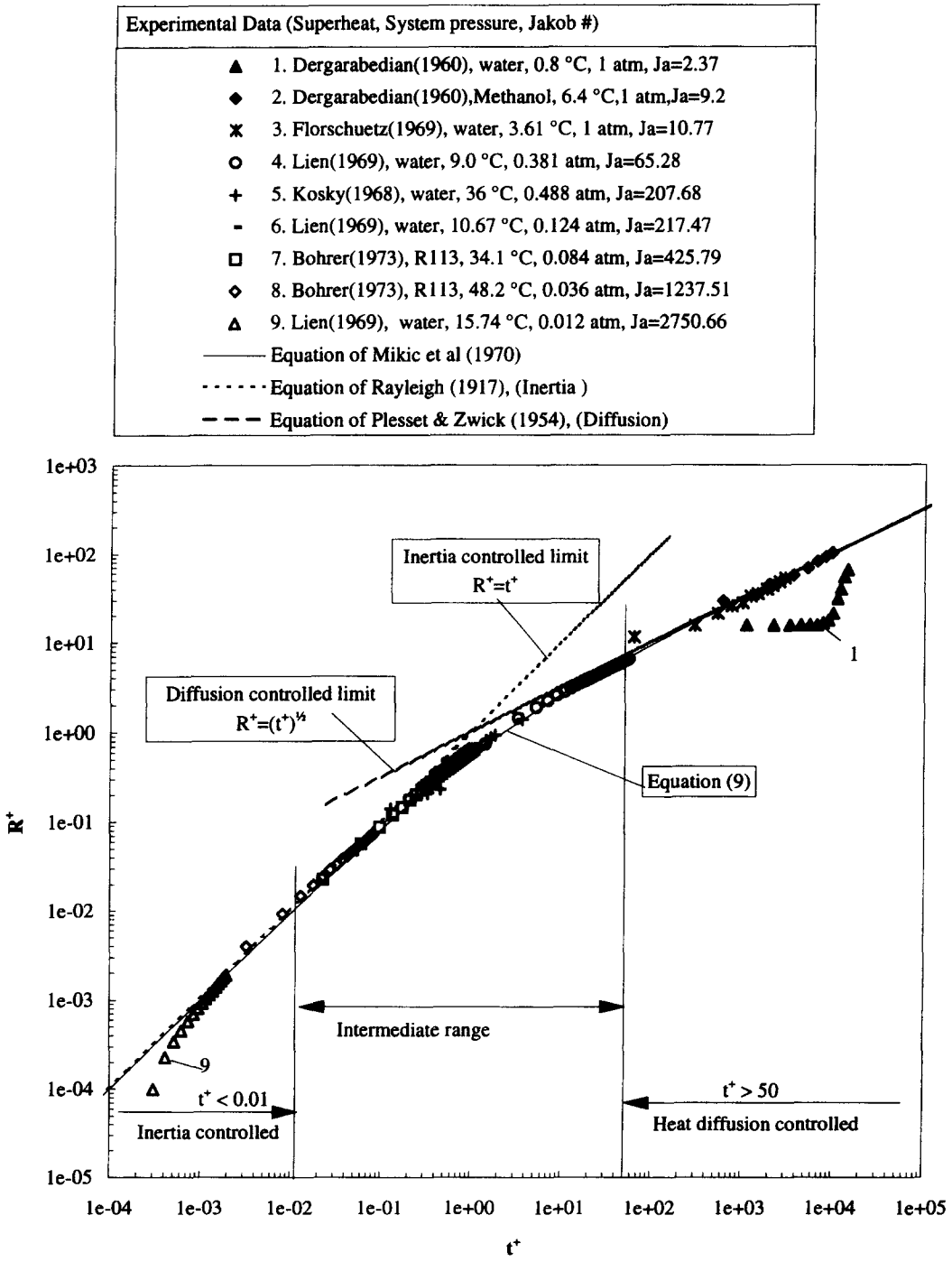

Fig. 14. Comparisons of various measurements of bubble growth with the analysis of Mikic *et al.* [11], and with limiting cases of inertia and heat diffusion controlled growth.

nate, the inertia controlled equation (7) and diffusion controlled equation (8) are superimposed on the solution of Mikic *et al.* [11], equation (9) in Fig. 14, along with experimental data for various fluids under a variety of conditions. The upper and lower limits are defined as those values of t^+ where a discrepancy of 10% exists between equations (7) and (8) and the solution of Mikic *et al.* [11]. Experiments designated by 1–3 in Fig. 14 are in the region of heat diffusion controlled growth, experiments 4–8 are in the region of the intermediate range, while experiment 9 is in the region of inertia controlled growth. Experiments 1 and 9 are seen to diverge from the solution of Mikic *et al.* [11], and are associated with respective surface tension and liquid inertia effects being significant during the early stages of bubble growth. Both of these behaviors are described quite well by the computational procedures presented here and by Lee [19].

5. CONCLUSIONS

The numerical procedure for spherical vapor bubble growth successfully describes the complete process from the thermodynamic critical state over the widest ranges of pressure and superheat encountered in experimental work.

The disturbance necessary to compute vapor bubble growth from the critical size does not significantly affect subsequent bubble growth except for very low levels of superheat, provided that the disturbance is sufficiently small, and manifests itself as a change in the bubble growth delay time. The delay time converges to a constant as the magnitude of the disturbance decreases. The early stages of the growth are governed by surface tension and liquid inertia, and becomes of significance as either the initial liquid superheat or system pressure decreases. The bubble growth tends to become inertia controlled as either the liquid superheat increases or the system pressure decreases, or tends to become heat diffusion controlled as either the liquid superheat decreases or the system pressure increases.

Except for the early stages of the bubble growth, the closed form solution of Mikic *et al.* [11] is in good agreement not only with the present numerical computations, but also with a wide variety of experimental results. The early stages involve both surface tension and liquid inertia, which complicate the predictions by analytical methods.

Acknowledgement—This work was conducted under NASA Contract NAS 3-25812. The dedicated interest and support of Dr Fran Chiaramonte and Mr Jack Salzman of the NASA Lewis Research Center are gratefully recognized.

REFERENCES

1. A. Prosperetti and M. Plesset, Vapor-bubble growth in a superheated liquid, *J. Fluid Mech.* **85,** 349–368 (1978).
2. Lord Rayleigh, *Phil. Mag.* **34,** 94 (1917).
3. M. S. Plesset and S. A. Zwick, The growth of vapour bubble in superheated liquid, *J. Appl. Phys.* **25,** 493 (1954).
4. P. Dergarabedian, The rate of growth of vapor bubbles in superheated water, *J. Appl. Mech.* **20,** 537–545 (1953).
5. H. K. Forster and N. Zuber, Growth of a vapor bubble in a superheated liquid, *J. Appl. Phys.* **25,** 474 (1954).
6. G. Birkhoff, R. S. Margulies and W. A. Horning, Spherical bubble growth, *Phys. Fluid* **1,** 201 (1958).
7. L. E. Scriven, On the dynamics of phase growth, *Chem. Engng Sci.* **1,** 1–13 (1959).
8. P. G. Kosky, Bubble growth measurements in uniformly superheated liquids, *Numer. Engng Sci.* **23,** 695–706 (1968).
9. L. W. Florschuetz, C. L. Henry and A. Rashid Khan, Growth rates of free vapor bubbles in liquids at uniform superheats under normal and zero gravity conditions, *Int. J. Heat Mass Transfer* **12,** 1465–1489 (1969).
10. Y. C. Lien, Bubble growth rates at reduced pressure, D.Sci. Thesis, MIT (1969).
11. B. B. Mikic, W. M. Rohsenow and P. Griffith, On bubble growth rate, *Int. J. Heat Mass Transfer* **13,** 657–666 (1970).
12. T. G. Theofanous and P. D. Patel, Universal relations for bubble growth, *Int. J. Heat Mass Transfer* **19,** 425–429 (1976).
13. T. H. Bohrer, Bubble growth in highly superheated liquids, M.S. Thesis, Chemical Engineering, Purdue University (1973).
14. T. Theofanous, L. Biasi and H. S. Isbin, A theoretical study on bubble growth in constant and time-dependent pressure fields, *Chem. Engng Sci.* **26,** 263–274 (1969).
15. S. J. Board and R. B. Duffey, Spherical vapor bubble growth in superheated liquids, *Chem. Engng Sci.* **26,** 263–274 (1971).
16. M. Dalle Donne and M. P. Ferranti, The growth of vapor bubble in superheated sodium, *Int. J. Heat Mass Transfer* **18,** 477–493 (1975).
17. M. S. Plesset and S. A. Zwick, A nonsteady heat diffusion problem with spherical symmetry, *J. Appl. Phys.* **23,** 95 (1952).
18. V. E. Skripov, *Metastable Liquids*, Chap. 2. Wiley, New York (1974).
19. H. S. Lee, Vapor bubble dynamics in microgravity, Ph.D. Thesis, The University of Michigan (1993).
20. P. Dergarabedian, Observations on bubble growth in various superheated liquids, *J. Fluid Mech.* **9,** 39–48 (1960).
21. E. M. Sparrow, S. Ramadhyani and S. V. Patankar, Effect of subcooling on cylindrical melting, *J. Heat Transfer* **100,** 395–402 (1978).
22. C.-J. Kim and M. Kaviany, A numerical method for phase-change problems, *Int. J. Heat Mass Transfer* **33,** 2721–2734 (1990).
23. S. V. Patankar, *Numerical Heat Transfer and Fluid Flow*. Hemisphere, Washington, DC (1980).

APPENDIX A. FORMULATION OF GOVERNING EQUATIONS

The major assumptions made in this work are:

(1) Bubble remains spherical.
(2) A uniform pressure and temperature exist within the vapor bubble.
(3) The vapor temperature inside the bubble is at the liquid–vapor interface temperature, $T_v = T_i$.
(4) The liquid is incompressible.

The momentum equation in spherical coordinates is given by:

$$\frac{\partial u}{\partial t} + u\frac{\partial u}{\partial r} = -\frac{1}{\rho}\frac{\partial P}{\partial r} + \frac{\mu}{\rho}\left(\frac{1}{r^2}\frac{\partial}{\partial r}\left(r^2\frac{\partial u}{\partial r}\right) - \frac{2\mu}{r^2}\right). \quad \text{(A1)}$$

The continuity equation with assumption (4) is given by:

$$\frac{\partial}{\partial r}(r^2 u) = 0. \tag{A2}$$

Using the continuity equation (A2) and integrating equation (A1) from the bubble surface (R) to infinity (∞), the momentum equation is written in terms of the bubble radius:

$$R\frac{d^2R}{dt^2} + \frac{3}{2}\left(\frac{dR}{dt}\right)^2 = \frac{P_R - P_\infty}{\varepsilon\rho_l} \tag{A3}$$

where

$$\varepsilon = \left(1 - \frac{\rho_v}{\rho_l}\right).$$

The balance of pressure across the liquid–vapor interface gives:

$$P_v(T) - P_R = \frac{2\sigma(T)}{R} + 4\frac{\mu}{R}\frac{dR}{dt} \tag{A4}$$

where P_R is the liquid pressure adjacent the bubble wall.

Inserting equation (A4) into equation (A3) yields

$$R\frac{d^2R}{dt^2} + \frac{3}{2}\left(\frac{dR}{dt}\right)^2 = \frac{P_v(T) - P_\infty}{\varepsilon\rho_l} - \frac{2\sigma(T)}{\varepsilon\rho_l R} - 4\frac{\mu}{\varepsilon\rho_l R}\frac{dR}{dt}. \tag{A5}$$

The initial conditions are:

$$R(0) = R_c \quad \text{and} \quad \frac{dR}{dt}(0) = 0 \text{ at } t = 0. \tag{A6}$$

The driving force for the bubble growth in equation (A5) is the pressure difference between the vapor bubble and the liquid adjacent the bubble, which is constrained by the surface tension. Equation (A5) implies that static equilibrium will exist when the first and second derivatives are zero. For the initial vapor bubble of critical size, this gives, since $T_v = T_\infty$ initially:

$$R_c = \frac{2\sigma(T)}{P_v(T) - P_\infty}. \tag{A7}$$

The energy equation in spherical coordinates is:

$$\frac{\partial T}{\partial t} + u_r\frac{\partial T}{\partial r} = \alpha\left(\frac{\partial^2 T}{\partial r^2} + \frac{2}{r}\frac{\partial T}{\partial r}\right) \tag{A8}$$

where

$$u_r = \varepsilon\frac{R^2}{r^2}\frac{dR}{dt}. \tag{A9}$$

The initial condition is:

$$T(r, 0) = T_\infty. \tag{A10}$$

The boundary conditions are: $T(\infty, t) = T_\infty$

$$4\pi R^2 k_l\left(\frac{\partial T}{\partial r}\right)_{r=R} = h_{fg}\frac{d}{dt}\left(\frac{4}{3}\pi R^3\rho_v\right). \tag{A11}$$

Equation (A11) is the heat balance at the bubble liquid–vapor interface. The bubble growth problem in a superheated liquid is solved by coupling equation (A5) and equation (A8), with the initial and boundary conditions given by equations (A6), (A10) and (A11), together with the vapor pressure relation.

APPENDIX B. NUMERICAL SOLUTION PROCEDURE

A program was written in Fortran to solve the transient spherical bubble growth problem in superheated liquids. The solution method uses the implicit finite difference method for the energy equation, with the explicit boundary condition given by equation (A11). An irregular grid is adopted for the liquid to minimize the computation time, with the grid spacing decreasing as the bubble interface is approached. 100 nodes were used for about 2 mm of the thermal boundary layer. The positions of the control volume faces are determined according to the relation:

$$\eta_i = \left(\frac{i-1}{n-1}\right)^p \quad i = 1, 2, 3 \ldots n \tag{B1}$$

where n is total number of control volume faces and p is an exponent suited to the problem, usually taken to be between 1 and 3. If $p = 1$, a regular grid results; if $p > 1$, an irregular grid results.

A small disturbance is necessary in order to initiate the bubble growth from the critical size, which is in metastable equilibrium. In this work, a small temperature disturbance is given once at the liquid–vapor interface, and thereafter the program runs without further disturbances.

A dimensionless coordinate (η) is introduced to immobilize the moving boundary, as given by Sparrow *et al.* [21], and referred to as the Landau coordinate:

$$\eta = \frac{r - R(t)}{\delta} \quad 0 \leqslant \eta \leqslant 1 \quad R(t) \leqslant r \leqslant R(t) + \delta \tag{B2}$$

where δ is an arbitrary distance which can be considered to correspond to a thermal boundary layer. The conservative forms of the continuity and the energy equation are used to begin the coordinate transformation.

$$\frac{\partial}{\partial t}(r^2\rho) + \frac{\partial}{\partial r}(\rho r^2 u) = 0 \tag{B3}$$

$$\frac{\partial}{\partial t}(r^2\rho h) + \frac{\partial}{\partial r}(\rho r^2 u h) = \frac{\partial}{\partial r}\left(r^2 k\frac{\partial T}{\partial r}\right). \tag{B4}$$

The transformation of the governing equations is facilitated by the following relations, also given by Sparrow *et al.* [21]:

$$\frac{\partial}{\partial r} = \frac{1}{\delta}\frac{\partial}{\partial \eta} \quad \frac{\partial}{\partial t} = \frac{\partial}{\partial t} - \frac{r'}{\delta}\frac{\partial}{\partial \eta} \tag{B5}$$

$$r' = \frac{\partial r}{\partial t}(\eta, t) = \eta\frac{d\delta}{dr} + \frac{dR}{dr}. \tag{B6}$$

The continuity and energy equations (B3) and (B4) can be transformed to the immobilized equations by using equations (B2), (B5) and (B6), as was done by Kim and Kaviany [22] based on the work of Sparrow *et al.* [21]. This has the significant effect of eliminating the convection term in equation (B4), with the result:

$$\frac{\partial}{\partial t}\left(\rho\frac{\partial V}{\partial \eta}\right) + \frac{\partial F}{\partial \eta} = 0 \tag{B7}$$

$$\frac{\partial}{\partial t}\left(\rho h\frac{\partial V}{\partial \eta}\right) + \frac{\partial J}{\partial \eta} = 0 \tag{B8}$$

where

$$F(\eta, t) = \rho\left(r^2 u - \frac{\partial V}{\partial t}\right) \tag{B9}$$

$$J(\eta, t) = F(\eta, t) - \frac{r^2 k}{\delta}\frac{\partial T}{\partial \eta} \tag{B10}$$

$$V(\eta, t) = \tfrac{1}{3} r^3 \tag{B11}$$

$$r(\eta, t) = \eta\delta + R(t). \tag{B12}$$

The term $F(\eta, t)$ and the term $J(\eta, t)$ represent the mass flux and the energy flux, respectively, across the face of the control volume.

Now, the transformed conservation equations (B7) and (B8) are discretized by using the implicit numerical scheme of Patankar [23]. For a typical control volume, the integration of equation (B8) with the aid of equation (B7) gives:

$$\alpha_P T_P = \alpha_E T_E + \alpha_W T_W + b \tag{B13}$$

where

$$\alpha_P = \alpha_E + \alpha_W + \alpha_P^0, \quad \alpha_P^0 = \frac{\rho c (\Delta V)_P^0}{\Delta t} \tag{B14}$$

$$\alpha_E = D_e A(|P_e|) + \max\{-cF_e, 0\} \tag{B15}$$

$$\alpha_W = D_w A(|P_w|) + \max\{-cF_w, 0\} \tag{B16}$$

$$D_e = \frac{r_e^2 k}{\delta(\Delta\eta)_e} \quad D_w = \frac{r_w^2 k}{\delta(\Delta\eta)_w} \quad P_e = \frac{cF_e}{D_e} \quad P_w = \frac{cF_w}{D_w} \tag{B17}$$

$$b = \alpha_P^0 T_P^0 \quad (\Delta V)_P = V_e - V_w \quad (\Delta V)_P^0 = V_e^0 - V_w^0 \tag{B18}$$

$$V_e = \tfrac{1}{3} r_e^3 \quad V_w = \tfrac{1}{3} r_w^3 \tag{B19}$$

$$r_e = \eta_e \delta + R(t) \quad r_w = \eta_w \delta + R(t). \tag{B20}$$

The various numerical schemes developed and used in recent years have been formulated as different choices of the function $A(|P|)$ in equations (B15) and (B16), as developed by Patankar [23], which amount to different means for expressing the derivatives between nodal points. The power law scheme suggested by Patankar [23] is used here:

$$A(|P_e|) = \max\{0, (1 - 0.1|P_e|)^5\} \tag{B21}$$

$$A(|P_w|) = \max\{0, (1 - 0.1|P_w|)^5\}. \tag{B22}$$

The max $\{B, C\}$ denotes the greater of B and C.

The previous value at time t is known and is denoted by using the superscript "o", while the new value at time $t + \Delta t$ is unknown and is denoted by using no superscript. The discretized equation (B13) can be solved efficiently by using TDMA (TriDiagonal Matrix Algorithm) with the two aforementioned boundary conditions equation (A11), which can be discretized considering the finite volume at the boundary:

$$\rho_l c_l A \frac{(\Delta r)_w}{2} \frac{T_W - T_W^0}{(\Delta t)} = kA \frac{T_P - T_W}{(\Delta r)_w} - h_{fg} \frac{d}{dt}\left(\frac{4}{3}\pi R^3 \rho_v\right) \tag{B23}$$

or

$$T_W = \frac{2F_0}{1 + 2F_0} T_P + \frac{T_W^0 - 2F_0 Q_{xk}}{1 + 2F_0} \tag{B24}$$

where

$$F_0 \equiv \frac{\alpha \Delta t}{(\Delta r)_w^2}, \quad Q_{xk} = \frac{h_{fg}(\Delta r)_w}{k} \frac{dR}{dt} \rho_v.$$

Equation (B24) is used as the discretized boundary condition for the energy equation, since dR/dt can be obtained from a time step solution of the momentum equation (A5) by using the Runge–Kutta method.

The computation of bubble growth is begun from the critical radius given by equation (A7) for the initial values of the bulk temperature (T_∞) and the system pressure (P_∞). A vapor temperature slightly higher than the initial bulk temperature, given by equation (12), is imposed for the initial time step to provide the disturbance necessary for growth from the critical size. This small disturbance does not affect the subsequent bubble growth except during the very early stages of bubble, and could be interpreted as a small statistical fluctuation of the local liquid temperature in the vicinity of the critical size vapor bubble. Once this disturbance is given, equation (A5) is solved by means of the Runge–Kutta method assuming that the pressure is constant for the short period of the time step, so that R, $\dot{R}$ and $\ddot{R}$ are produced. The $\dot{R}$ is used to solve equation (A11), the boundary condition at the liquid–vapor interface. The discretization equation for equation (A8) is then solved by means of the TDMA so that a new interface temperature (T_i) is determined, which then is used to obtain the vapor pressure corresponding to the interface temperature with assumption (3) in Appendix A. This process is iterated to update the temperature variation until the velocity difference between the time step $(i-1)$ and (i) converges to zero. The convergence is so fast that only two or three iterations are usually required to satisfy the convergence limit. The actual time required is dependent upon how the time step variation is arranged. Although the implicit scheme is generally described as stable, a realistic solution does not necessarily follow for sufficiently large time steps. In the present work, a time step of 10^{-8} s, determined empirically, is employed initially and increased as bubble growth takes place. As stated earlier, a maximum of 100 nodes were used for the maximum thermal boundary layer thickness of about 2 mm. Details of the numerical scheme are give in Lee [19].